



## NANOLITHOGRAPHICALLY DEFINED MAGNETIC STRUCTURES

Stephen Y. Chou, Peter R. Krauss, Mark S. Wei,  
and Paul B. Fischer

Department of Electrical Engineering  
University of Minnesota, Minneapolis, MN 55455

### Introduction

Coercivity, coercive squareness and many other magnetic properties of a magnetic material strongly depend upon the geometric factors of the magnetic grains in the material, such as the grain size and anisotropy, the grain magnetization orientation, and the spacing between the grains. In a conventional as-deposited magnetic film, the geometric factors generally have a broad distribution and therefore cause local variation of magnetic properties. To develop new materials for ultra-high density magnetic recording and to obtain a better understanding of magnetic behavior of a material, it is desirable to precisely control these geometric factors. Conventional methods for attempting to obtain such control include optimization of film deposition conditions, alloying, epitaxial growth and deposition on amorphous or crystal substrates, introduction of stacking faults, and insertion of nonmagnetic material between the magnetic grains. However, none of these approaches can precisely control the geometric factors.

As nanofabrication technology advances, it is now possible to accurately control the geometric factors of magnetic grains in a thin film using nanolithography. These nanolithographically-defined magnetic materials open up new opportunities for engineering novel magnetic materials, developing ultra-high density magnetic storage, exploring limits of magnetic storage, and understanding the fundamentals of magnetics.

In this paper we review our work in fabrication of nanomagnetic structures using electron beam nanolithography and other nanofabrication technologies, characterization of these structures using magnetic force microscope (MFM) and possible applications. Particularly, we will discuss: (1) isolated and interactive nanoscale single-domain Ni bars that have a width varying from 15 to 200 nm and a spacing from 100 nm to 2  $\mu\text{m}$ ; (2) arrays of single-domain Ni pillars that have a uniform diameter of 35 nm, a height of 120 nm, and a density of 65 Gbits/in<sup>2</sup>--over two orders of magnitude greater than state-of-the-art magnetic storage density; (3) a new paradigm for ultra-high density magnetic recording media: quantum magnetic disk; (4) a ultra-high resolution single-domain MFM tip.

### Isolated and Interactive Nanomagnetic Bar Arrays

Nanoscale ferromagnetic bars are a simple and important magnetic structure. Previously, a joint team from the University of California at San Diego and IBM studied lithographically-defined nanoscale permalloy bars [1,2]. In that study, isolated bars had a fixed length of 1  $\mu\text{m}$  and a fixed width of 133 nm; interactive bar arrays had a fixed spacing with the strongest coupling along the bars' long axis. To further understand the effects of geometric factors, we studied isolated and interactive nanoscale Ni bars with various widths and



Figure 1. SEM image of a high aspect ratio isolated Ni bar that is 1  $\mu\text{m}$  long and 15 nm wide.

spacings, which were interactive along bar's short axis. All the bars are 35 nm thick. For isolated bars, the bar length was fixed at 1  $\mu\text{m}$ , the spacing between bars was 10  $\mu\text{m}$ , and the bar width varied from 15 to 200 nm. Figure 1 shows a scanning electron micrograph of a Ni bar with a 15 nm width and an average edge variation of 4 nm. For interactive bar arrays, the bar width and length were fixed at 100 nm and 1  $\mu\text{m}$ , respectively. The spacing between bars along the long axis was 2  $\mu\text{m}$ , but the spacing between the bars along the short axis varied from 200 to 600 nm. Figure 2 shows a large array of Ni bars which are 20 nm wide, 200 nm long, and 250 nm apart along the short axis and 100 nm apart along the long axis. These isolated and interactive nanomagnetic nickel bars were fabricated using electron beam nanolithography and a lift-off process [3, 4].

The nanomagnetic bars were studied using a custom built MFM that was modified from a commercial atomic force microscope (AFM). These MFM measurements showed that for bars of a width smaller than 150 nm, the virgin magnetic state is single domain with magnetization along the direction of its easy (i.e. long) axis; and, the bars of wider width are multi-domain.

The magnetization switching field of an isolated bar was found to be a strong function of width, as shown in Figure 3. As the bar width decreases from 200 to 55 nm, the switching field increases from 100 to 740 Oe, which is, to our best knowledge, the highest switching field reported for Ni. This field is also about 30 times larger than the coercivity of the Ni film that was evaporated at the same time during the bar's fabrication. The increase in switching field is due to the larger switching energy required by a larger anisotropy. However, as the bar width decreases further below 55 nm, the switching field starts decreasing due to thermal effect.

The interactive bar arrays studied by MFM have a bar width of 100 nm and a spacing between bars of 0.2, 0.4, and 0.6  $\mu\text{m}$  respectively along the short axis. Figure 4 shows a MFM image of an interactive array. The

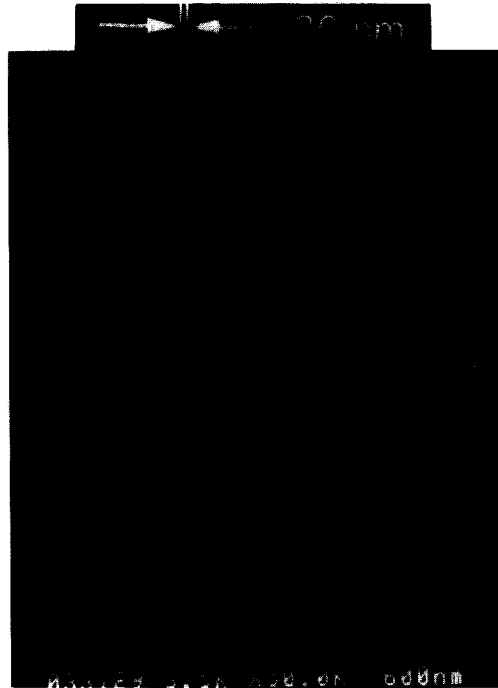


Figure 2. SEM image of interactive bar arrays. Each bar is 20 nm wide, 200 nm long, and 35 nm thick.

switching field vs. the bar spacing was measured and is shown in Figure 5. In this measurement, an average of about 30 bars were counted for each data point and the bars at the end of each row were not counted. Figure 5 shows three facts. First, smaller spacing results in a smaller switching field. The switching field for a 100 nm wide isolated bar is 300 Oe. But due to interaction, the mean value of the switching field (i.e. the field at which 50% of bars can flip) is 205, 232, and 260 Oe for a spacing of 0.2, 0.4, and 0.6  $\mu\text{m}$  respectively. Second, the switching field decreases almost linearly with the reduction of spacing at a rate 15 Oe per 100 nm. This behavior is due to the fact that as the spacing decreases, the demagnetization field generated by neighboring bars increases and will help a bar to flip. Third, the switching field has a distribution of about 100 Oe which is due to bar interaction as well as size variations.

### Ultra-high Density Nanomagnetic Pillar Arrays

To study the vertical magnetic recording, arrays of Ni pillars on silicon were fabricated using electron beam nanolithography and electroplating. The details of the fabrication are reported elsewhere [4]. As shown in Figure 6, the pillars have a uniform diameter of 35 nm, a height of 120 nm, and a period of 100 nm; therefore, the density of the pillar arrays is 65 Gbits/in<sup>2</sup>--over two orders of magnitude greater than the state-of-the-art magnetic storage density.

We have attempted to use a high resolution magnetic force microscope (MFM) to examine these ultra-high density pillar arrays, but were unsuccessful. The primary reason is that since the topology image and magnetic image are intertwined in MFM, the aspect ratio of our nanomagnetic pillars is so large that the topology image

### Effect of Bar Width on Switching Field

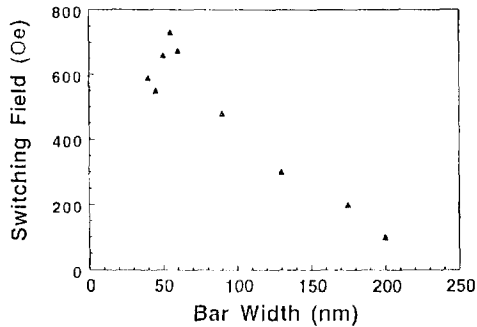


Figure 3. Switching field of isolated bars vs. bar width. The maximum switching field is 740 Oe for 55 nm wide bars. The bars are 1  $\mu\text{m}$  long and actual bar width was measured using SEM.

completely masks the magnetic image. Despite the difficulty in characterizing these nanomagnetic pillars, MFM measurements showed that horizontal nanomagnetic bars of 35 nm thickness and nanoscale widths that were electroplated using the same technology as that for pillars are single domain, consistent with our theoretical estimation that the nanomagnetic pillars should be single-domain as well [5].

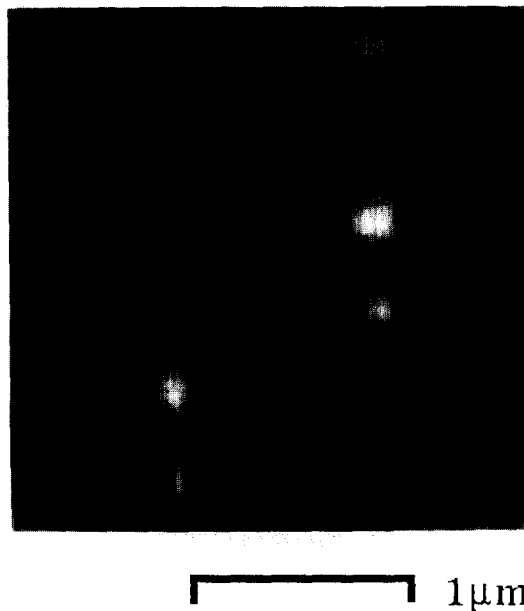


Figure 4. MFM image of one-dimensional interactive bar arrays with 400 nm spacing, 1  $\mu\text{m}$  long, and 100 nm wide. The black spot represents the north pole and the white spot represents the south pole.

### Effect of Bar Spacing on Switching Field

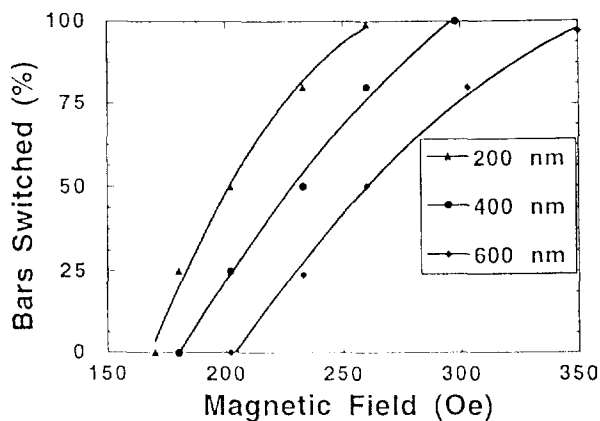


Figure 5. Percentage of bars that switched vs. the applied magnetic field for interaction bars with a spacing along the short axis of 200, 400, and 600 nm.

### Quantum Magnetic Disks

Based on these artificially-patterned single-domain magnetic structures, we propose a new paradigm for ultra-high density magnetic disk: Quantum Magnetic Disk (QMD) [6]. As shown in Figure 7, a quantum magnetic disk consists of pre-patterned single-domain magnetic structures embedded in a nonmagnetic disk. Each bit in the quantum magnetic disk is represented by a prefabricated single domain magnetic structure that has a uniform and well-defined shape, a pre-specified location, and, most importantly, a quantified magnetization that has only two states: the same in value and opposite in direction. In other words, the shape, magnetization, and location for each bit in a quantum magnetic disk are all quantized and pre-defined during the disk

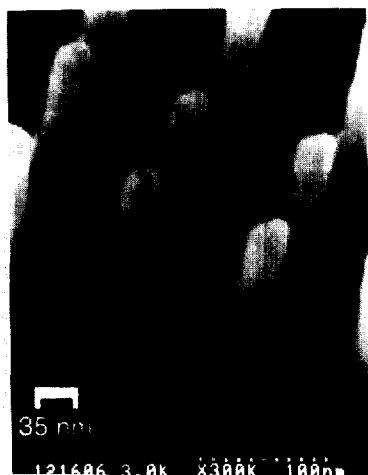


Figure 6. SEM image of Ni pillar array of 35 nm diameter, 120 nm height, and a 100 nm spacing. The density is 65 Gbits/in<sup>2</sup> and the aspect ratio is 3.4.

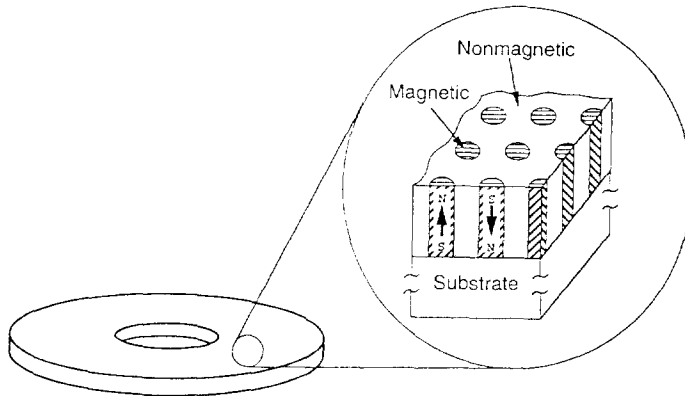


Figure 7. Schematic of a quantum magnetic disk which consists of pre-patterned single-domain magnetic structures embedded in a nonmagnetic disk. Only the vertical magnetization is shown, but the disk can be made with longitudinal magnetization.

manufacturing. On the contrary, in a conventional magnetic disk where a bit is not defined at disk fabrication, the shape and magnetization of each bit have a broad distribution and the location of a bit can be anywhere on disk. The QMD also differs from the discrete track disk [7, 8] and the discrete segment disk [9, 10] where the magnetization (both value and direction) of each bit can have a continuous and broad distribution.

The advantages of quantum magnetic disks over the conventional disks are apparent. First, the writing process in the quantum disk is greatly simplified, resulting in much lower-noise and less error rate and allowing much higher density. In the quantum disk, the writing process does not define the location, shape, and magnetization value of a bit, but just simply flips the quantized magnetization orientation of a pre-patterned single-domain magnetic structure. The writing can be perfect, even though the head slightly deviates from the intended bit location and partially overlaps with other bits, as long as the head flips only the magnetization of the intended bit. But in the conventional magnetic disk, the writing process must define the location, shape, and magnetization of a bit. If the head deviates from the intended location, the head will write part of the intended bit and part of the neighboring bits.

Second, the quantum disk can track every bit individually, but the conventional disk cannot track all of its bits. This is because in the quantum disk each bit is separated from others by nonmagnetic material, but in the conventional disk many bits are connected. The individual-bit-tracking ability allows precise positioning, less error rate, and therefore ultra-high density storage.

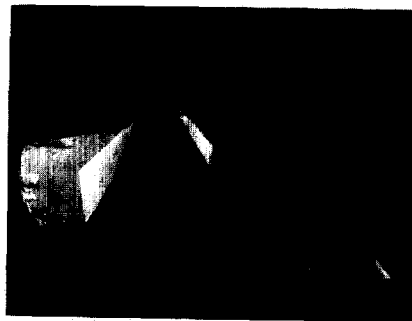


Figure 8. Completed SMS tip with a nanoscale nickel magnetic sensor at the tip. The Ni spike, which is trough shaped with a tapered end, is 30 nm thick, ~150 nm wide, 1.4  $\mu\text{m}$  long, and has a 10 nm tip radius. The non-magnetic contamination pillar is ~150 nm wide and 1.7  $\mu\text{m}$  long. Intrinsic stress in evaporated Ni bends the tip.

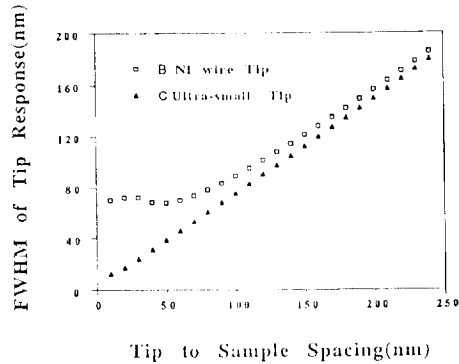


Figure 9. FWHM response of the SMS and Ni wire tips to a magnetic dipole for different values of tip-to-sample spacing.

Finally, reading in the quantum disk has much less jitter than that in the conventional disk. The reason is that in the conventional disk the boundary between bits is ragged and not well defined, but in the quantum disk, each bit is defined with nanometer precision (can be less than the grain size) and is well separated from each other.

### Ultra-high Resolution Magnetic Force Microscope Tip

The MFM tip is one of the most important elements in determining the resolution and sensitivity of an MFM. Previously, sharpened Ni wires [11] and magnetically coated atomic force microscope tips [12] have been used as MFM tips. Such tips suffer from several drawbacks, such as poor spatial resolution due to multiple magnetic domains, broad distribution of magnetic charge as well as strong stray field, and a large magnetic charge that can alter the magnetic properties of the magnetic material under inspection.

We have proposed and fabricated a novel magnetic force microscope tip referred to as single-domain magnetic spike (SMS) tip that consists of a  $\sim 30$  nm thick ferromagnetic film coated on one side of a non-magnetic pillar which is  $\sim 150$  nm wide and over  $1.5 \mu\text{m}$  long as shown in Fig. 8 [13]. The pillar was grown on the apex of a commercial scanning force microscope tip using high-resolution contamination electron beam lithography operated at 35 kV voltage and 10 pA beam current. The ferromagnetic film such as nickel and cobalt, was evaporated on the pillar from an angle so that only the pillar, not the rest of the tip, was coated.

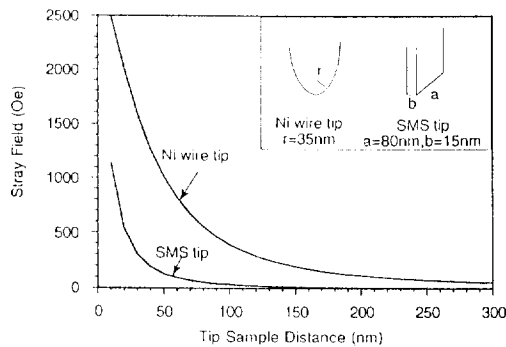


Figure 10. Stray field of SMS and Ni wire tips.

The coated ferromagnetic film has a trough shape and a tapered end with a tip radius of  $\sim 10$  nm. The film is single domain because of the nanoscale size and shape anisotropy. Compared to conventional Ni wire tips, the new tips offer better imaging resolution because of a much smaller effective magnetic cross section at the end of the tip, and thus have a lower stray field because of its small magnetic charge making them well suited to measuring soft magnetic materials.

Calculations were performed to evaluate the performance of the SMS tips. Figure 9 shows the FWHM response of the SMS and Ni wire tips to a magnetic dipole vs. the tip-to-sample spacing. For tip-to-sample spacings greater than about 100 nm, the responses of the two tips are similar. At a tip-to-sample spacing of 20 nm, however, the FWHM response of the SMS tip is nearly 20 nm, whereas the Ni wire tip is still  $\sim 70$  nm. This demonstrates that the ultimate resolution of an MFM tip is limited by its size. The calculation assumes the SMS tip to be rectangular with a thickness of 15 nm, width of 80 nm, and a tip length of 1  $\mu\text{m}$ , and the Ni wire tip to be cylindrical with a radius of 35 nm and a length of 1  $\mu\text{m}$ . In both cases, the magnetization was assumed to be parallel to the tip's axis due to shape anisotropy.

Another advantage of the SMS tip is a smaller stray field compared to a conventional Ni wire tip as shown in Fig 10. The greatly reduced volume of magnetic material of the SMS tip results in a stray field of only 150 Oe at a distance of 50 nm, making the SMS tip better suited for studying soft magnetic material. Although conventionally coated tips in general also have a stray field smaller than that of a Ni wire tip due to a reduced magnetic volume [14], the SMS tips offer at least a 50% further reduction.

### **Conclusion**

Using nanolithography-based fabrication technology, we can engineer magnetic structures with magnetic properties that cannot be achieved by conventional methods. Undoubtedly the nanofabrication approach opens up new opportunities for engineering novel magnetic materials, developing ultra-high density magnetic storage, exploring limits of magnetic storage, and understanding the fundamentals of magnetism.

### **Acknowledgment**

We would like to thank J.G. Zhu for stimulating discussion, Hao Fang for MFM measurements, and Bob Guibord for his technical assistance in fabrication. This work was supported in part by ARPA, ONR, the Packard Foundation through a Packard Fellowship to SYC, and the AFOSR through an Air Force Laboratory Graduate Fellowship to PBF.

### **References**

1. J.F. Smyth, S. Schultz, D.R. Fredkin, T. Koehler, I.R. McFaydlin, D.P. Kern and S.A. Rishton, *J. of Appl. Phys.*, 63(8), pt. 2B, 4237 (1988).
2. G.A. Gibson, J.F. Smyth, S. Schultz, and D.P. Kern, *IEEE Trans. Magn.*, 27(6), 5187 (1991).
3. S.Y. Chou and P. Fischer, *J. Vac. Sci. Technol.*, B8(6), 1919 (1990).
4. P.R. Krauss, P.B. Fischer, and S.Y. Chou, *J. Vac. Sci. Technol.*, B12(6), 3639 (1994).
5. A. Aharoni, *J. Appl. Phys.* 63, 5879 (1988).
6. S.Y. Chou, private communication, May, 1994.
7. L.F. Shew, *IEEE Trans., Broadcast Tel. Receivers*, BTR-9, 56 (1963).
8. S.E. Lambert, I.L. Sander, A.M. Pattlach, and M. T. Krounbi, *IEEE Trans. on Magn.*, MAG-23, 3690 (1987).
9. K.A. Belser, T. Makansi, and I.L. Sanders, US Patent No. 4,912,585, March 27, 1990.
10. S.E. Lambert, I.L. Sanders, A.M. Pattan, M.T. Krounbi, and S.R. Hetzler, *J. Appl. Phys.* 69(8), 4724 (1991).
11. Y. Martin and H. K. Wickramasinghe, *Appl. Phys Lett.*, 50, 1455 (1987).
12. Y. Honda, S. Hosaka, A. Kikugawa, S. Tanaka, Y. Matsuda, M. Suzuki and M. Futamoto, *Jpn. J. Appl. Phys.*, 31, L1061 (1992).
13. P.B. Fischer, M.S. Wei, and S.Y. Chou, *J. Vac. Sci. Technol.*, B 11(6), 2570 (1993).
14. P. Bryant, S. Schultz and D. R. Fredkin, *J. Appl. Phys.*, 69, 5877 (1991).